CARBON 52 (2013) 137–144

Available at www.sciencedirect.com

SciVerse ScienceDirect

journal homepage: www.elsevier.com/locate/carbon

Energy loss distribution of proton beams at normal incidence on multi-walled carbon nanotubes

Jorge E. Valdés [a,b,c], Carlos Celedón [a,d], Rodrigo Segura [e], Isabel Abril [b,*], Rafael Garcia-Molina [f], Cristian D. Denton [b], Néstor R. Arista [d], Patricio Vargas [a]

[a] Departamento de Física – Laboratorio de Colisiones Atómicas, Centro para el Desarrollo de la Nanociencia y la Nanotecnología, Centro de Nanociencia de Valparaíso, Universidad Técnica Federico Santa María (UTFSM), Valparaíso 2390123, Chile
[b] Departament de Física Aplicada, Universitat d'Alacant, E-03080 Alacant, Spain
[c] Donostia International Physics Center (DIPC), P. Manuel de Lardizabal 4, E-20018 San Sebastián, Spain
[d] Centro Atómico Bariloche, División Colisiones Atómicas, RA-8400 S.C. de Bariloche, Argentina
[e] Departamento de Química y Bioquímica, Facultad de Ciencias, Universidad de Valparaíso, Chile
[f] Departamento de Física – Centro de Investigación en Óptica y Nanofísica, Universidad de Murcia, E-30100 Murcia, Spain

ARTICLE INFO

Article history:
Received 27 April 2012
Accepted 8 September 2012
Available online 17 September 2012

ABSTRACT

The irradiation with energetic proton beams impinging normal to the axis of a multi-walled carbon nanotube (MWCNT) is studied both experimentally and theoretically, in the 2–10 keV energy range. The MWCNTs are dispersed on top of a very thin film of holey amorphous carbon (a-C) substrate. Measurements of the proton energy loss distribution are performed after MWCNT irradiation with energetic proton beams by the transmission technique. The resulting energy loss spectra in the forward direction show two well differentiated peaks, whose origin is elucidated by using a semi-classical simulation of the proton trajectory through the nanotube. We found that the experimental lower-energy loss peak mostly comes from protons travelling between the outer walls of the MWCNT, whereas the high-energy loss peak is mainly due to protons that interact with the MWCNTs just on top of the supporting a-C substrate.

1. Introduction

Carbon nanotubes (CNTs) are systems of unquestionable technological interest. Due to their low dimensionality, nanometer size and remarkable electronic, mechanic and magnetic properties, nanotubes are promising structures for many purposes in several fields of physics, materials science, or biomedicine [1]. Among their remarkable applications it is worth to highlight their use in nanoelectronics (nanotube field effect transistors, CNT-based nonvolatile memory, quantum-effect devices or sensors), in computing and data storage, in chemical detectors, or ion storage [2]. CNTs are also useful to manufacture materials with high mechanical resistivity, such as tips for AFM or nanoelectrodes for optical devices [3].

The bombardment of carbon nanotubes with energetic particles (ions or electrons) is a well-established method to modify their structure and their physical properties in a controlled way with quasi-atomic precision. Changes in the electronic [4], mechanical [5] and magnetic [6] properties of the irradiated CNTs have been reported. Therefore, a possible route to design nanotube-based circuitry and achieving the desired functionality of the electronic devices is to use energetic particle beams to modify the structure, the morphology, and the local electronic properties of nanotubes in a convenient and determinate manner, creating defects or by doping

* *Corresponding author:* Fax: +34 965909726.
E-mail address: ias@ua.es (I. Abril).
0008-6223/$ - see front matter
http://dx.doi.org/10.1016/j.carbon.2012.09.014

with alien atom species. So, to exploit all the advantages of the irradiation-assisted engineering, a complete atomic-scale understanding of the response of nanotubes to irradiation is required. In the last few years a significant experimental and theoretical advance has been made in the study of the effects of ion irradiation on CNTs, as shown in recent reviews [7–9].

The majority of ion bombardment studies refer to slow heavy ion effects on CNTs, were the elastic interactions of the projectile with the carbon atoms prevail and the main effects of irradiation are the creation of local defects, doping, functionalization, amorphization, straightening, cutting, as well as joining and welding of CNTs [9]. However the interest in the irradiation of this type of structures with light ions, such as protons, has increased in the last years [10]. One of the reasons of this interest is the expected use of nanotubes in outer space, where high-energy protons are abundant and can produce a degradation of CNT-based electronic devices [11].

In addition, Krasheninnikov and co-workers [12] have emphasized the role of electronic excitations in ion collisions with CNT, since their effects are generally less destructive and reversible that the nuclear collisions and due to their significance in mediating ionic interactions even in the low-energy regime.

Although the feasibility of ion beams to induce controlled changes in the properties of CNTs has been widely discussed, no work has been devoted to consider the possibilities of ion beams as analytical tools to characterize their structure and morphology, such as the number of walls constituting the nanotube, which is one of the parameters that strongly affect their chemical and physical properties [13,14].

We study in this work, both experimentally and by a semiclassical simulation, the irradiation of multi-walled carbon nanotubes (MWCNTs) by a proton beam impinging perpendicularly to their main axis. The projectile energy is taken in the keV range of energies, where the electronic stopping regime dominates. The experimental setup and the proton energy-loss distribution measurements are presented in Section 2. The main aspects of the simulation are discussed in Section 3, whereas the results obtained are presented in Section 4, which are linked to a qualitative discussion in Section 5 about the origin of the peaks found in the experimental energy-loss distribution of the transmitted protons detected in the forward direction. Finally, the most important conclusions are summarized in Section 6.

2. Experiment

Multi-walled carbon nanotube (MWCNT) samples were prepared at the Departamento de Física at UTFSM by following the procedure described in [15] and [16]. The MWCNTs were synthesized by thermal chemical vapour deposition (CVD) in a horizontal tube furnace, where 0.01 g of Pd(1%)/γ-Al_2O_3 catalyst was annealed up to 800 °C with a stream of Ar (200 cm^3/min) and H_2 (100 cm^3/min) and kept at this temperature by 10 min. Then, acetylene (40 cm^3/min) was added to the furnace during 30 min at 800 °C, while the Ar/H_2 stream was kept at the same rate. In such conditions acetylene is catalytically decomposed to yield the nanotubes and finally the catalyst is carefully removed to obtain purified MWCNT samples [17].

In order to characterize the samples and perform ion energy loss measurements, the MWCNTs were dispersed on a sample holder consisting in a holey amorphous carbon coated copper grid (3 mm diameter). Fig. 1 depicts a TEM micrograph of the resulting MWCNTs, taken with a FEI Tecnai G2 F20 S-Twin microscope operated at 200 kV. This high resolution image shows details about the graphitic walls and the empty channel of the nanotubes, whose average inner and outer diameters are 5 and 27 nm, respectively. It is worth to notice how a sizeable amount of MWCNTs is on top of the amorphous carbon (a-C) supporting grid, which is 18 nm thick, whereas the remainder rests on the grid holes.

The ion energy loss measurements were performed at Laboratorio de Colisiones Atómicas, UTFSM. The proton beam was obtained from a hot discharge ion source, after which it was focused by an electrostatic lens system, being mass selected by a Wien velocity filter. The system detection consisted in an MCP detector plus electronic devices. The energy of the projectiles was analyzed by means of a spherical electrostatic analyzer having a resolution less than 1%. In this manner, an associated error less than 3% was obtained in the energy loss determination. The collision chamber was maintained at a pressure of 10^{-8} to 10^{-7} Torr during the experiment. The measurements were performed in transmission geometry with 2–10 keV proton beams hitting the nanotubes perpendicular to its main axis. It is pointed out that overlapping of carbon nanotubes does not introduce detectable signals in the recorded energy spectrum. This is so because the proton spectrum resulting from stacked MWCNTs have an extremely weak intensity (due to the extra angular deflection), being practically undetectable with our present experimental set up.

We show in Fig. 2 the experimental energy loss distribution measured in the forward direction of a 10.1 keV proton beam bombarding the MWCNTs supported on the holey a-C film (full squares). In the same figure also is shown, just to

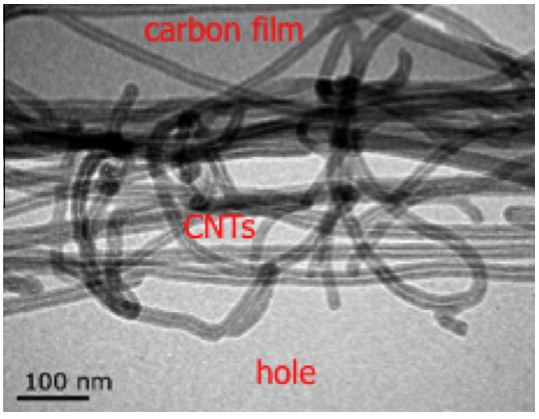

Fig. 1 – Transmission electron microscopy micrograph of MWCNTs dispersed on a holey amorphous carbon coated TEM grid, as prepared to be bombarded by the proton beam. Notice that a sizeable part of the MWCNTs is resting on top of an a-C film (shown partially in the upper half of the picture).

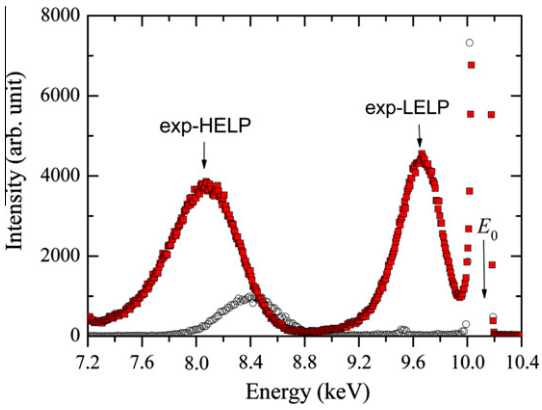

Fig. 2 – Experimental proton energy distribution in the forward direction after a proton beam with initial energy E_0 = 10.1 keV interacts with MWCNTs supported on an a-C grid (full squares) and with an amorphous carbon film (empty circles).

indicate energy position, the energy loss peak corresponding to protons after traversing the 18 nm-thick a-C substrate (empty circles), which was measured in a separated experiment. In all the incident energy range studied in this work (2–10 keV) the experimental energy loss distribution of protons traversing the MWCNT shows two distinct peaks, to which we will refer as high-energy loss peak (exp-HELP) and low-energy loss peak (exp-LELP). In the figure E_0 denotes the proton beam initial energy.

In Fig. 3 we show the difference between the experimental proton beam initial energy E_0 and the high-energy loss peak ($\Delta E_{\text{exp-HELP}}$) by empty square symbols and with the low-energy loss peak ($\Delta E_{\text{exp-LELP}}$) by empty round symbols, for protons interacting with the MWCNTs supported on the a-C holey grid, as a function of E_0. The energy difference $\Delta E_{\text{peaks}} = E_{\text{exp-HELP}} - E_{\text{exp-LELP}}$ between the exp-HELP and exp-LELP peaks appearing in the energy loss distribution is also depicted in Fig. 3 by full triangles. ΔE_{peaks} divided by the a-C thickness of 18 nm is shown in the inset (full triangles) and compared with available stopping power experimental data from [19–21] and density functional calculations [22] for amorphous carbon.

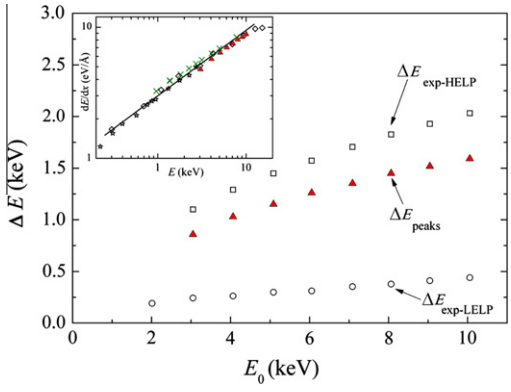

Fig. 3 – Difference between the initial proton beam energy E_0 and the experimental energy loss for the two peaks, exp-HELP (empty squares) and exp-LELP (empty circles) appearing in the proton energy distribution at the forward direction after interacting with MWCNTs supported on the a-C holey grid, as a function of the incident energy E_0. The difference between the energy of the two peaks in the proton energy distribution $\Delta E_{\text{peaks}} = E_{\text{exp-HELP}} - E_{\text{exp-LELP}}$ is also depicted by full triangles. The inset shows that ΔE_{peaks} divided by the a-C thickness satisfactorily agrees with the experimental data from [19] (empty diamonds), [20] (empty starts), [21] (crosses) and with density functional calculations [22] (solid line) for amorphous carbon.

The inset of Fig. 3 shows the excellent agreement of the measured "peak-energy differences" divided by the film thickness when compared to the experimental stopping power data and theoretical calculations for a-C films, which clearly indicates that the experimental exp-HELP is the consequence of a shift in the exp-LELP due to protons interacting with the supporting a-C film after crossing the MWCNTs.

In what follows we will elucidate the origin of the exp-LELP and the justification of the exp-HELP by performing a detailed simulation of the projectile motion through MWCNTs, in the conditions reported in the experiment.

3. Simulation

In this section we introduce the main features of the simulation used to analyze the irradiation of a MWCNT by an energetic proton beam. A scheme of the system under study is shown in Fig. 4. The projectile, with initial energy E_0 around few keV, impinges perpendicularly to the MWCNT axis, with an impact parameter b (randomly chosen in the simulation). In this energy range, the projectile energy loss is due mainly to the excitation of the target valence electrons [23,24], while the energy loss due to elastic scattering with the target nuclei can be neglected if we consider only those protons emerging in the forward direction. As the energy transfer due to elastic collisions in this energy range is not enough to create defects in the nanotubes [9], in our simulation we will consider that the nanotube structure is not altered by the proton irradiation.

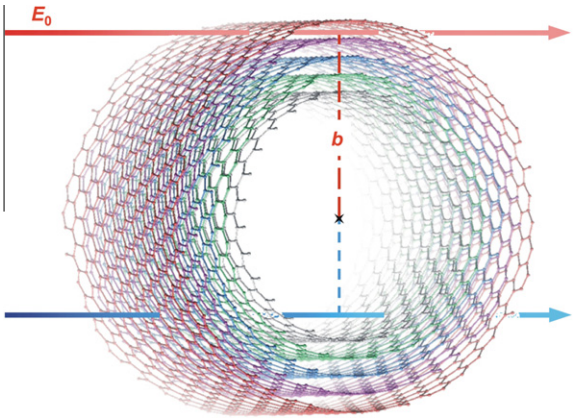

Fig. 4 – Diagram of a proton beam that impinges perpendicularly to the main axis of a MWCNT. The initial proton energy is E_0 and b is the impact parameter. Two representative impact parameters are shown.

The nanotube is made of concentric tubes (hereafter referred to as walls) composed of carbon atoms. Each wall can be described as a graphene sheet rolled into a cylindrical shape, whose structure exhibits axial symmetry and, in general, a spiral conformation, called chirality [25]. The chirality parameters (n_i, m_i) of each wall determine its diameter D_i through the relation: $D_i = \frac{\sqrt{3}}{\pi} L_{C-C} \sqrt{n_i^2 + m_i^2 + n_i\, m_i}$, where $L_{C-C} = 0.142$ nm is the carbon–carbon bond length [25]. The distance between adjacent walls in the MWCNT has been found to be close to the interlayer distance in graphite, i.e. 0.335 nm [26]. The study with microscopy techniques of a MWCNT can determine its inner and outer diameter or its number of walls, but does not provide information about the chirality of its walls. In order to construct the structure of a MWCNT for our simulation we choose arbitrary values of (n_1, m_1) for the inner wall according to the value of the inner diameter. For the rest of the walls we use the algorithm $(n_{i+1}, m_{i+1}) = (n_i{+}7, m_i{+}3)$ [27], which ensures the correct distance between adjacent walls.

The trajectory of each proton through the nanotube is obtained by solving numerically its classical equation of motion [18] with the velocity form of the Verlet algorithm [28,29]. In what follows we briefly describe the procedure. Knowing the position $\vec{r}$, the velocity $\vec{v}$ and the total force $\vec{F}$ that act on the projectile at a given time t, it is possible to calculate its new position and velocity after a time step Δt:

$$\vec{r}(t+\Delta t) = \vec{r}(t) + \vec{v}(t)\Delta t + \frac{1}{2}\frac{\vec{F}(t)}{M}(\Delta t)^2, \quad (1)$$

$$\vec{v}(t+\Delta t) = \vec{v}(t) + \frac{1}{2}\frac{(\vec{F}(t) + \vec{F}(t+\Delta t))}{M}\Delta t, \quad (2)$$

where M is the mass of the proton. Through an iterative process, we are able to follow the trajectory of the projectile, obtaining its energy and direction after it exits the MWCNT.

The forces acting on the protons are due both to inelastic interactions with the MWCNT electrons and to elastic processes with carbon nuclei. In our range of projectile energies, the energy transfer to valence electrons generates a retarding friction force $\vec{F}_{stop}$, which produces the energy loss of the protons. We assume that during each time step the proton is slowed down as if it were travelling in a nearly free electron gas with a density n, equal to the local electronic density felt by the proton at each position when moving through the MWCNT; this approach corresponds to the local density approximation (LDA). As we will see later, this local electronic density has a strong spatial variation and so the retarding force will vary considerably depending on the region of the nanotube where the projectile moves. Besides the stopping (inelastic) force $\vec{F}_{stop}$, the protons also experience repulsive (elastic) forces with the target nuclei, which we obtain as $\vec{F}_{elast} = -\vec{\nabla} V(\vec{r}, \vec{R})$, where $V(\vec{r}, \vec{R})$ is a Thomas–Fermi–Molière type interaction potential between a proton and a carbon nuclei; the interested reader is referred to Ref. [18] for further details. In the simulation, the time step Δt was chosen to be approximately 2×10^{-18} s in order to properly map the inhomogeneous electronic density of the MWCNTs.

Due to the stochastic character of the inelastic processes, the electronic stopping force $\vec{F}_{stop}$ on a proton with velocity v is mapped from a Gaussian distribution, where its mean value is the stopping power, S, and its standard deviation is related to the energy-loss straggling, Ω^2, which accounts for the fluctuations in the energy loss. Namely:

$$\vec{F}_{stop} = -[S + (\Omega/\sqrt{v\Delta t})\ \sqrt{-2\ln\xi_1}\cos(2\pi\xi_2)]\ \ \hat{v}, \quad (3)$$

where ξ_1 and ξ_1 are random numbers uniformly distributed between 0 and 1, and the factor $\sqrt{-2\ln\xi_1}\cos(2\pi\xi_2)$ comes from the Box–Muller transformation that gives a Gaussian distribution [30].

In order to calculate the values of S and Ω^2 entering in the above equation, which describe the electronic energy loss of a moving proton, we use the non-linear density functional theory (DFT) for a free electron gas. In this formalism the electronic stopping power S is proportional to the proton velocity v, $S = Q(n)v$ [22], whereas the energy-loss straggling Ω^2 is proportional to the square of the velocity, $\Omega^2 = W(n)v^2$ [31]. Both the stopping coefficient $Q(n)$ and the straggling coefficient $W(n)$ depend on the electronic density n of the free electron gas.

The electronic density of the MWCNT is approximated by the sum of the electronic density of each nanotube wall, which can be obtained by rolling the electronic density of a graphene sheet according to the corresponding chirality parameters of the wall. This is a good approximation as long as the wall diameter is not too small, because then the curvature is small enough to consider that carbon atoms up to second and third nearest neighbours in the graphene sheet are coplanar. We use the electronic density of a graphene sheet obtained through the *ab initio* TB-LMTO method which, despite using the atomic-sphere approximation for the one-electron potential, provides a charge density in excellent agreement with the one obtained from a linear augmented plane-wave full-potential calculation [32–34]. Fig. 5 shows the mean electronic density in a plane parallel to a graphene sheet, as a function of its distance to the sheet; the inset depicts the local electronic density around the carbon atoms. The strong localization of the electronic density near the graphene sheet guarantees that there is not overlapping between electronic densities of the adjacent walls, because the distance between nanotube walls is 0.335 nm.

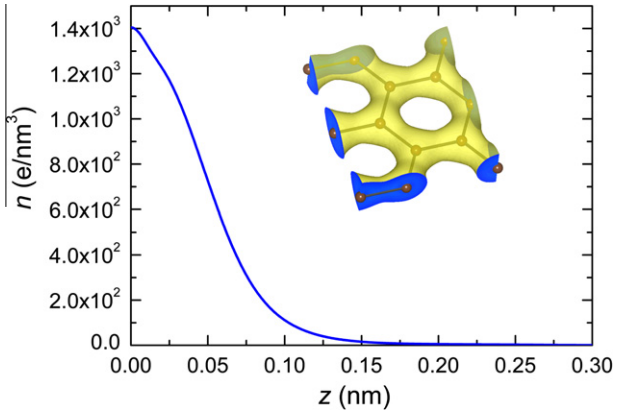

Fig. 5 – Mean electronic density in a plane, parallel to a graphene sheet, as a function of the perpendicular distance z to the sheet, obtained by the *ab initio* TB-LMTO model [32,33]. The inset shows the isosurface for the electronic density around the carbon atoms of graphene whose value is around 1350 e/nm^3.

The simulation indicates that protons moving through a wall will span regions with large electronic densities, whereas protons travelling between adjacent walls will found rather small electronic densities. This fact will affect the resulting energy loss of the protons after interacting with the MWCNT, according to the kind of trajectories they follow.

On the other hand, the elastic interactions of the proton with carbon nuclei of the MWCNT mainly affect their direction of motion. We model these elastic interactions by including in the simulation a repulsive force calculated with the empirical Thomas–Fermi–Molière type potential [35]. The energy loss due to the elastic collisions is neglected since it is small compared with the electronic energy loss in the range of energies discussed in this work [23]. Due to the mass difference between protons and carbon atoms, we assume that the recoil of the nanotube atoms can be neglected and so, the MWCNT structure can be considered as fixed [9].

4. Results of the simulation

In what follows we present and discuss the results obtained from the simulation of the irradiation of a 10 keV proton beam impinging perpendicularly to the axis of a MWCNT, for different impact parameters b, as sketched in Fig. 4. The MWCNT taken for the simulation has internal diameter $D_{int} = 5$ nm, so we have chosen the chirality parameters $(n_1, m_1) = (64, 1)$. The number of walls was chosen to be 33, which gives an external diameter $D_{ext} \cong 27$ nm. These values characterizing the MWCNT were taken in accordance with our previous work [16], but the results we will obtain can be easily generalized to other geometrical parameters. Simulations were done by randomly choosing the impact parameter and rotating the MWCNT around its axis. The results presented in what follows are the average of 10^7 histories.

In Fig. 6 we show the energy distribution (normalized to unity area) of the exiting protons after interacting with the MWCNT. The grey dotted curve corresponds to all protons that cross the nanotube. In that case a peak around 8.4 keV is clearly visible, whereas a small shoulder is observed at ~9.7 keV. However if we examine the energy distribution of the protons exiting in a cone of one degree with respect to the initial beam direction (represented by the solid curve), two distinct peaks can clearly be seen at the same energies than in the previous case, where the more intense one corresponds to protons losing smaller energies. Besides, we observe that the low-energy loss peak (sim-LELP) grows at expenses of the high-energy loss peak (sim-HELP). These two peaks in the energy distribution only appear when the simulation collects particles located at around zero degree with respect to the initial beam direction (within a cone of 0.5° semiangle), disappearing as the angular width covered by the detector widens.

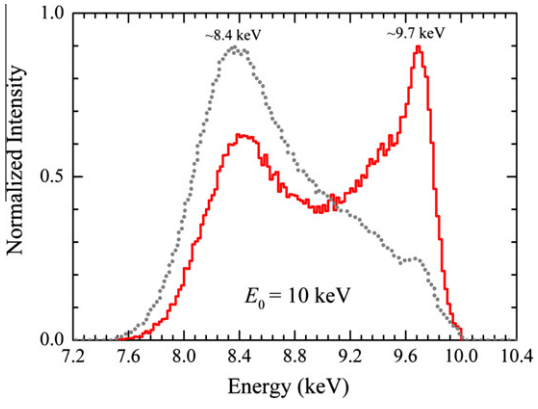

Fig. 6 – Simulated energy distribution of protons leaving the MWCNT in the forward direction within a cone of 0.5° semiangle (solid line) and in all directions (grey dotted line). The distributions are normalized to unity area. The initial proton energy is 10 keV and the MWCNT has 33 shells, with internal and external diameters of 5 and 27 nm, respectively.

In order to interpret the origin of the simulated peaks shown in Fig. 6 for the proton energy distribution detected in the forward direction within a 0.5° semiangle cone, we analyse the distribution of impact parameters b corresponding to protons exiting in the forward direction, which is depicted in Fig. 7. As can be observed, most of the cases correspond to protons with large impact parameters, which imply that these protons have crossed the MWCNT near its outer border. The strong reduction of protons with small and intermediate impact parameters means that in these cases the projectiles experience relatively large angular deflection, being removed from the forward direction, whereas those with high values of b practically cross the MWCNT without suffering deviation from their initial direction. It is important to notice that the distribution depicted in Fig. 7 shows peaks at specific values of impact parameters, which correspond to situations where protons move between adjacent external walls and therefore experience soft collisions with carbon atoms. On the other side, protons impinging with small impact parameters need to go through the MWCNT walls, thus having a larger probability of hard collisions with carbon atoms and experiencing an enhanced multiple scattering.

To estimate the origin of the protons that arrive to the detector, we relate the impact parameter distribution of the

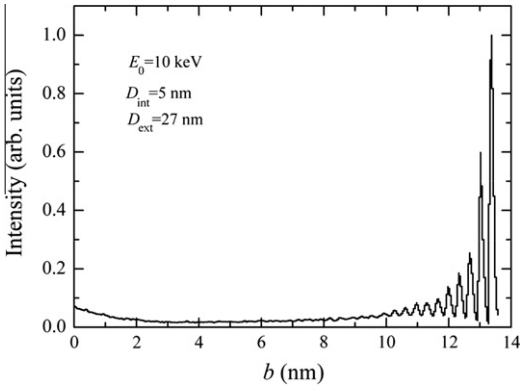

Fig. 7 – Distribution of the impact parameters b contributing to protons exiting in the forward direction within a cone of 0.5° semiangle. The initial proton energy is 10 keV and the MWCNT has 33 shells, with internal and external diameters of 5 and 27 nm, respectively.

protons with the peaks appearing in the energy distribution depicted in Fig. 6. We show in Fig. 8 with a black curve the impact parameter distribution of the simulated histories where protons exit the MWCNT in the forward direction (±0.5°) with energies between 8.25 and 8.75 keV, which determine the limits of the main contribution to the simulated high energy-loss peak (sim-HELP). The grey curve in Fig. 8 illustrates the same but for histories where protons exit with energies between 9.5 and 10 keV, which is the major contribution to the low energy-loss peak (sim-LELP). We can observe that the sim-HELP is due to protons incident with small and intermediate impact parameters, a situation in which the MWCNT thickness is larger. Nevertheless, taking aside this geometric factor, at small and intermediate impact parameters protons have to go through the MWCNT walls traversing high electronic density areas (see Fig. 5); this yields a large energy loss on those protons going through walls. On the other hand, the histories contributing to the sim-LELP correspond to protons with large impact parameters, as the grey curve in Fig. 8 shows, where the very sharp peaks indicate that the impact parameters related to the sim-LELP correspond to protons incident between the more external walls. These protons move between adjacent walls where the electronic density is small (see Fig. 5) and, therefore, losing only a small part of its energy.

Therefore, from the simulation we conclude that the majority of protons leaving the sample in the forward direction with negligible deflection and small energy loss are those that had a trajectory near the edge of the MWCNTs. Consequently these protons have a larger probability to reach the detector at zero angle with small energy loss. Although these protons represent a minority with respect to the total number of protons that interact with the MWCNT, most of them will arrive to the detector in comparison with those projectiles that cross wider MWCNT regions and suffer higher angular deflections due to the larger multiple scattering.

We have also analyzed the effect of changing the number of walls of the MWCNT in the energy distribution of the exiting protons. Fig. 9 shows the energy distribution of a 10 keV proton beam exiting in the forward direction (±0.5°) after interacting with a MWCNT of internal diameter 5 nm and different number of walls (from 5 up to 30 walls). For all the MWCNT studied here the position of the sim-LELP is almost independent of the number of walls of the MWCNT, since it is due to those protons that travel between its outer walls. On the contrary, the mean energy-loss of the sim-HELP increases with the number of walls of the MWCNT. This is consistent with the fact that the sim-HELP is due to protons of small impact parameter, going through the walls of the nanotube, and experiencing in their trajectories higher electronic densities.

Fig. 10 shows the proton mean energy-loss $\Delta E_{\text{sim-HELP}}$ of the high energy-loss peak (sim-HELP) in the forward direction

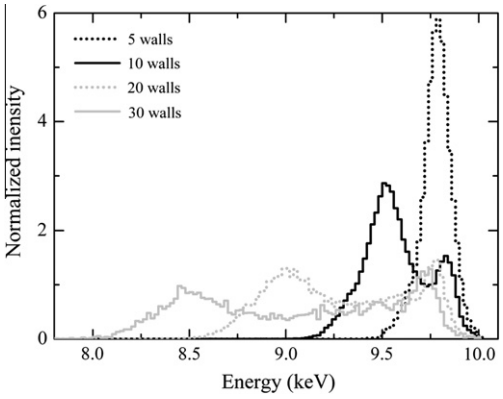

Fig. 9 – Energy distributions of a proton beam with initial energy E_0 = 10 keV exiting in the forward direction within a cone of 0.5° semiangle after interacting with MWCNT with different number of walls. The distributions are normalized to unity area. The internal diameter of the MWCNT remains unchanged (D_{int} = 5 nm) but the external diameter changes according to the number of walls.

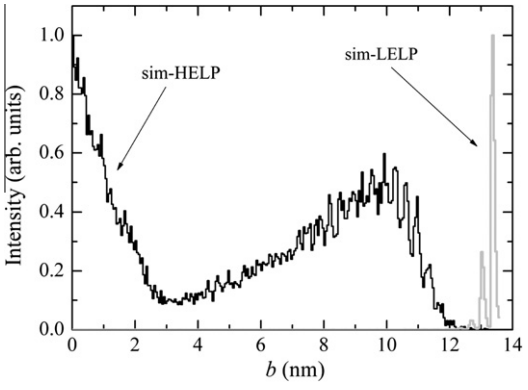

Fig. 8 – Distribution of the impact parameters *b* that give rise to protons exiting in the forward direction within a cone of 0.5° semiangle. Solid line represents the contribution to the sim-HELP for transmitted protons with energies between 8.25 and 8.75 keV. Grey line corresponds to the sim-LELP for proton energies from 9.5 to 10 keV. The simulation parameters are the same than in Fig. 6.

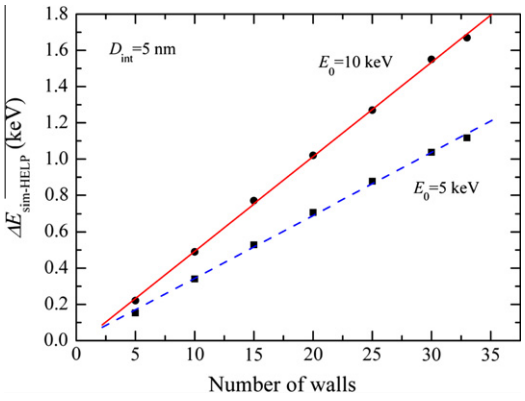

Fig. 10 – Mean energy-loss of the high energy-loss peak (sim-HELP) found in the energy distributions at zero angle (±0.5°) of protons interacting with a MWCNT, as a function of the number of walls of the nanotube. The initial energy of the proton beam is 10 keV (circle-symbols and solid line) and 5 keV (square-symbols and dashed line). The internal diameter of the MWCNT is 5 nm.

(±0.5°) as a function of the number of walls of the nanotube. The linear relation depicted in the figure means that $\Delta E_{\text{sim-HELP}}$ is proportional to the number of walls, with the proportionality factor being 52 eV/wall for a 10 keV proton beam and 34.7 eV/wall for a 5 keV proton beam. Besides, from these simulations we obtain the mean energy loss of a proton beam after traversing a graphene sheet, which in our case corresponds to 26 eV for 10 keV protons and 17.4 eV for 5 keV protons (i.e., half of the value corresponding to each cylindrical wall).

5. Comparison between experiment and simulation

When confronting the experimental energy distribution (Fig. 2) with the simulated one (Fig. 6) for a proton beam with initial energy $E_0 \simeq 10$ keV we can see that a peak appears in both cases at 9.7 keV, whereas the experimental 8 keV peak (Fig. 2) does not match with the peak at 8.4 keV obtained in the simulation.

The former peak corresponds to the low-energy-loss peak (LELP) discussed in Section 4, being mostly due to protons bombarding the MWCNT with large impact parameters and therefore moving through adjacent outer walls, resulting in small energy losses, as discussed previously.

However, the sim-HELP obtained in the simulation does not agree with the one appearing in the experimental distribution exp-HELP. To understand qualitatively the origin of the experimental peak at 8 keV we need to take into account that protons moving *through* the MWCNT (i.e., those interacting with small impact parameters) cross most of the MWCNT walls and therefore experience more collisions with the target carbon atoms, producing more angular deflection than those travelling between the external walls. As the proportion of holes in the supporting grid is smaller than the a-C area, a sizeable amount of protons exiting the MWCNT have to pass through the a-C supporting film, where additional energy loss as well as elastic scattering takes place. The larger angular deflection of protons contributing to the HELP peak prevents many of them from reaching the detector, which explains the relative heights of both, HELP and LELP, peaks.

Those protons that entered the a-C supporting film coming from the central part of the MWCNT (i.e., those that produce the sim-HELP in the simulated distribution) have more angular dispersion than the ones coming from the borders of the MWCNT (i.e., those that produce the sim-LELP in the simulated distribution). Therefore, the additional angular dispersion experienced through the a-C film removes the formers from the forward direction, whereas the latter group is still able to reach the detector located in the forward direction (with a detecting cone of 0.5° semiangle). The protons moving through the external walls of the MWCNT enter the a-C supporting film with an average energy of 9.7 keV and, after traversing the a-C film, they suffer an extra energy loss due to the interaction with the 18 nm thick amorphous carbon film. According to the ~9 eV/Å stopping power of a-C for 9.7 keV protons shown in the inset of Fig. 3, this energy loss amounts to ~1600 eV, which corresponds to the energy difference of the experimental peaks (cf. Fig. 2).

We conclude that the experimental energy distribution of protons in the forward direction after traversing MWCNTs supported on an a-C holey grid target results solely from protons which did travel through the more external adjacent walls. One of the peaks (exp-LELP) comes from MWCNTs lying on the holes of the grid, whereas the other peak (exp-HELP) originates mainly in the MWCNTs supported on the a-C substrate.

6. Summary and conclusions

The irradiation of MWCNTs by proton beams with energies around keV has been done experimentally and by simulation. The proton energy-loss distribution measurements were performed with MWCNTs supported on holey a-C by the transmission technique. The simulation followed the trajectories of each projectile by solving its classical equation of motion, where the electronic stopping force was accounted for by a non-linear density functional formalism depending on the local electronic density.

Two peaked proton energy distributions at the forward direction were obtained in the experiment as well as in the simulation. The low-energy-loss peak has a common origin in both cases, being due to protons moving through the most external walls of the MWCNTs. The high-energy-loss peak obtained in the simulation is due to protons that move through the central part of the MWCNT, and therefore lose more energy; but this peak does not appear in the experimental energy distribution because these protons suffer larger angular dispersion than those that crossed the MWCNTs through their most external adjacent walls, and therefore are removed from the forward direction after suffering additional angular dispersion when traversing the a-C film that makes the supporting holey grid. However, due to the small angular dispersion of the protons with larger impact parameter, they can reach the detector at zero angle after traversing the a-C film, with only an extra energy loss that shifts to a lower energy their energy distribution.

Therefore, the experimental energy distribution has its origin in the protons that did travel through adjacent external walls of the MWCNTs and that pass through the holes (the exp-LELP) or through the supporting a-C film (the exp-HELP).

Nevertheless, an important amount of energy is delivered to the MWCNT by those protons moving through the central part of the nanotube, which although not reflected in the energy distributions should be taken into account in order to consider possible damage effects in the carbon nanotubes.

Acknowledgements

This work has been financially supported by the following Grants: Fondecyt 1100759 and USM-DGIP 11.11.11, Financiamiento Basal para Centros Científicos y Tecnológicos de Excelencia (CEDENNA) and Project FIS2010-17225 by the Spanish Ministerio de Ciencia e Innovación. We thank Pablo de Vera for useful discussions.

REFERENCES

[1] Bauchman RH, Zakhidov AA, de Heer WA. Carbon nanotubes – the route toward applications. Science 2002;297:787–92.
[2] Dresselhaus MS, Dresselhaus G, Avouris P, editors. Carbon nanotubes, synthesis, structure, properties and applications. Berlin: Springer; 2001.
[3] Lidorikis E, Ferrari AC. Photonics with multiwall carbon nanotube arrays. ACS Nano 2009;3:1238–48.
[4] Gómez-Navarro C, de Pablo PJ, Gómez-Herrero J, Biel B, Garcia-Vidal FJ, Rubio A, et al. Tuning the conductance of single-walled carbon nanotubes by ion irradiation in the Anderson localization regime. Nat Mater 2005;4:534–9.
[5] Kis A, Csányi G, Salvetat J-P, Lee T-N, Couteau E, Kulik AJ, et al. Reinforcement of single-walled carbon nanotube bundles by intertube bridging. Nat Mater 2004;3:153–7.
[6] Talapatra S, Ganesan PG, Kim T, Vajtai R, Huang M, Shima M, et al. Irradiation-induced magnetism in carbon nanostructures. Phys Rev Lett 2005;95:097201-1–4.
[7] Miskovic ZL. Ion channelling through carbon nanotubes. Radiat Eff Defects Solids 2007;162:185–205.
[8] Miskovic ZL. Interactions of ions with carbon nanostructures. J Phys Conf Ser 2008;133:012011-1–012011-11.
[9] Krasheninnikov AV, Nordlund K. Ion and electron irradiation-induced effects in nano structured materials. J Appl Phys 2010;107:071301-1–071301-70.
[10] Emfietzoglou D, Kyriakou I, Garcia-Molina R, Abril I, Kostarelos K. Analytic expressions for the inelastic scattering and energy of electron and proton beams in carbon nanotubes. J Appl Phys 2010;108:054312-1–5.
[11] Hong W, Lee C, Nepal D, Geckeler KE, Shin K, Lee T. Radiation hardness of the electrical properties of carbon nanotube network field effect transistors under high-energy proton irradiation. Nanotechnology 2006;17:5675–80.
[12] Krasheninnikov AV, Miyamoto Y, Tomanek D. Role of electronic excitations in ion collisions with carbon nanostructures. Phys Rev Lett 2007;99:016104-1–4.
[13] Yang HS, Zhang L, Dong XH, Zhu WM, Zhu J, Nelson BJ, et al. Precise control of the number of walls formed during carbon nanotube growth using chemical vapor deposition. Nanotechnology 2012;23:065604-1–6.
[14] Shi X, Jiang B, Wang J, Yang Y. Influence of wall number and surface functionalization of carbon nanotubes on their antioxidant behavior in high density polyethylene. Carbon 2012;50:1005–13.
[15] Segura RA, Tello A, Cárdenas G, Häberle P. Synthesis of carbon nanotubes and nanofibers by decomposition of acetylene over a SMAD palladium catalyst. Phys Stat Sol A 2007;204:513–7.
[16] Kyriakou I, Celedón C, Segura R, Emfietzoglou D, Vargas P, Valdés JE, et al. Energy loss of protons in carbon nanotubes: experiments and calculations. Nucl Instrum Methods Phys Res B 2010;268:1781–5.
[17] Balasubramanian K, Burghard M. Chemically functionalized carbon nanotubes. Small 2005;1:180–92.
[18] Chen L, Shen J, Valdés JE, Vargas P, Esaulov VA. Energy loss of keV fluorine ions scattered off a missing-row reconstructed Au(110) surface under grazing incidence. Phys Rev A 2011;83:032901-1–032901-10.
[19] Arkhipov EP, Gott YuV. Slowing down of 0.5–30 keV protons in some materials. Sov Phys JETP 1969;29:615–8.
[20] Overbury SH, Dittner PF, Datz S, Thoe RS. Energy loss, angular distributions and charge fractions of low energy hydrogen transmitted through thin carbon films. Radiat Eff Defects Solids 1979;41:219–27.
[21] Serkovic LN, Sánchez EA, Grizzi O, Eckardt JC, Lantschner GH, Arista NR. Stopping power of fluorides for low-velocity protons. Phys Rev A 2007;76:0409011–4.
[22] Echenique PM, Nieminen RM, Ritchie RH. Density functional calculation of stopping power of an electron gas for slow ions. Solid State Commun 1981;37:779–81.
[23] Sigmund P. Particle penetration and radiation effects. General aspects and stopping of swift point charges. In: Springer series in solid-state sciences, vol. 151. Berlin: Springer; 2006.
[24] Ziegler JF, Biersack JP, Ziegler MD. The stopping and range of ions in matter. Version 2008. Code available from: http://www.srim.org.
[25] Saito R, Dresselhaus G, Dresselhaus MS. Physical properties of carbon nanotubes. London: Imperial College Press; 2004.
[26] Reich S, Thomsen C, Maultzsch J. Carbon nanotubes: basic concepts and physical properties. Berlin: Wiley-VCH; 2004.
[27] Ruland W, Schaperb AK, Houa H, Greinera A. Multi-wall carbon nanotubes with uniform chirality: evidence for scroll structures. Carbon 2003;41:423–7.
[28] Swope WC, Andersen HC, Berens PH, Wilson KR. A computer simulation method for the calculation of equilibrium constants for the formation of physical cluster of molecules: application to small water clusters. J Chem Phys 1982;76:637–50.
[29] Allen MP, Tildesley DJ. Computer simulation in liquids. Oxford: Oxford Science Publications; 1987.
[30] Box GEP, Muller ME. A note on the generation of random normal deviates. Ann Math Stat 1958;29:610–1.
[31] Puska MJ, Nieminen RM. Atoms embedded in an electron gas: phase shifts and cross sections. Phys Rev B 1983;27:6121–8.
[32] Andersen OK, Jepsen O. Explicit, 1st-principles tight-binding theory. Phys Rev Lett 1984;53:2571–4.
[33] Andersen OK, Jepsen O, Gloetzel D. In: Bassani F, Fumi F, Tosi MP, editors. Highlights of condensed matter theory. New York: North-Holland; 1985. p. 59–176.
[34] Andersen OK, Pawlowska Z, Jepsen O. Illustration of the linear-muffin-tin-orbital tight-binding representation: compact orbitals and charge density in Si. Phys Rev B 1986;34:5253–69.
[35] Eckstein W. Computer simulation of ion–solid interactions. Berlin: Springer-Verlag; 1991. p. 40–63.